IUST Iran University of Science and Technology

Iranian Journal of Electrical and Electronic Engineering

Journal Homepage: ijeee.iust.ac.ir

Research Paper

The Effect of Magnet Width and Iron Core Relative Permeability on Iron Pole Radii Ratio in Spoke-Type Permanent-Magnet Machine: An Analytical, Numerical and Experimental Study

A. Jabbari*(C.A.) and F. Dubas**

Abstract: In this paper, we present a mathematical model for determining the optimal radius of the iron pole shape in spoke-type permanent-magnet (PM) machines (STPMM) in order to minimize the pulsating torque components. The proposed method is based on the formal resolution of the Laplace's and Poisson's equations in a Cartesian pseudo-coordinate system with respect to the relative permeability effect of iron core in a subdomain model. The effect of PM width on the optimal radius of the iron pole has been investigated. In addition, for initial and optimal machines, the effect of the iron core relative permeability on the STPMM performances was studied at no-load and on-load conditions considering three certain PM widths. Moreover, the effect of iron pole shape on pulsating torque components with respect to certain values of iron core relative permeability was studied by comparing cogging torque, ripple and reluctance torque waveforms. In order to validate the results of the proposed analytical model, three motors with different PM widths were considered as case studies and their performance results were compared analytically and numerically. Two prototype spoke-type machines were fabricated and the experimental results were compared to analytical results. It can be seen that the analytical modeling results are consistent with the numerical analysis and experimental results.

Keywords: Analytical Model, Pulsating Torque Components, Iron Pole Shape Optimization, Finite Iron Core Relative Permeability, Quasi-Cartesian Coordinates, Subdomain Technique, Experimental Validation.

1 Introduction

SPOKE-TYPE Permanent-Magnet Machines (STPMMs) are considered as a good alternative to surface-mounted PM machines. Therefore, as with other PM machines, the elimination or reduction of pulsating torque components in these machines is of great importance [1, 2]. One of the effective methods for reducing pulsating torque in STPMMs is to optimize the shape of the rotor's iron pole. Various methods have been presented to determine the optimal shape of an iron pole in a STPMM. Most of the presented methods are based on numerical methods, especially the finite-element method (FEM). According to the author's knowledge, a mathematical relation has not been presented yet to determine the optimal radius of an iron pole in a STPMM. The effect of PM width and iron core relative permeability on the optimal radius of an iron pole and the machine performance have not been investigated.

Generally, numerical methods can be used to estimate the magnetic field in STPMMs. But using these methods is time-consuming. Therefore, providing analytical models for calculating machine performance

Iranian Journal of Electrical and Electronic Engineering, 2021.
Paper first received 31 January 2020, revised 11 April 2020, and accepted 21 April 2020.
* The author is with the Mechanical Engineering Department, Arak University, Arak, Iran.
E-mail: jabbari@araku.ac.ir.
** The author is with the Département ENERGIE, FEMTO-ST, CNRS, Université Bourgogne Franche-Comté, F90000 Belfort, France.
E-mail: fdubas@gmail.com.
Corresponding Author: A. Jabbari.
https://doi.org/10.22068/IJEEE.17.2.1802

in the initial design and optimization stages is of great importance. Several analytical studies have been carried out to calculate the magnetic vector potential in electric machines. Among the presented analytical models, the models based on Maxwell-Fourier methods are very accurate in comparison with the FEM. In most of these models, the performance characteristics of the machine are determined by the assumption that the iron core is infinitely permeable. In [2], authors have proposed an integrated method to optimize the rotor iron pole shape. They used the reduced basis technique coupled by FEM in order to reduce the enormous number of design parameters in rotor shape optimization process. A good comparison between the effect of shape optimization method and skew method on pulsating torque components and the STPMMs performance was studied in [3]. It has been stated that the iron pole shape optimization method in comparison with the stator slot skew method has a more favorable effect on the performance of the STPMM, especially the reduction of pulsating torque. Considering radial force harmonics in PM synchronous machines, the electromagnetic noise phenomenon was studied in [4]. The effect of static, dynamic, and mixed eccentricity in aspects of radial force and vibration was studied in [5]. In [6], by using magneto-mechanical coupled analysis, the magnetically induced vibration of an STPMM was mitigated. An analytical study was used to predict the electromagnetic performances and unbalanced magnetic forces in fractional slot STPMMs [7]. Semi-analytical harmonic models were presented for electric machine analysis considering magnetic saturation [8] and finite soft-magnetic material permeability [9]. Nonlinear analytical prediction of magnetic field and electromagnetic performances in switched reluctance machines was performed in [10]. A new subdomain technique was presented in [11] for electromagnetic performances calculation in radial-flux electrical machines considering finite soft-magnetic material permeability. Pole shape optimization of PM synchronous motors using the reduced basis technique was studied in [12]. A 2-D analytical model was used in order to estimate magnetic vector potential in surface-mounted/-inset PM machines in [13, 14], both in a pseudo-Cartesian coordinate system. In [15, 16], analytical modeling of magnetic field distribution was carried out in inner rotor brushless PM segmented surface-inset PM machines and multiphase H-type stator core PM flux switching machines, respectively. An analytical expression was derived in [17] for PM shape optimization in surface-mounted PM machines. An analytical study on iron pole shape optimization in high-speed interior PM machines was also performed in [18]. A new subdomain method for performances computation in interior PM machines taking into account iron core relative permeability was studied in [19]. Some overviews of analytical models were investigated in [20, 22] for analysis and design purposes PM electrical machines. new scientific contributions on the 2-D subdomain technique were presented in Cartesian [22] and polar [23] coordinates taking into account of iron parts. An analytical model was presented in order to predict the performances in PM machines including the diffusion effect [24]. Two-dimensional analytical calculation of magnetic field and electromagnetic torque was carried out for surface-inset PM motors [25] and STPMMs [26]. A 2-D analytical model for prediction of electromagnetic performances in STPMMs was presented in [27]. Nonlinear analytical calculation of magnetic field and torque of switched reluctance machines was studied in [28, 29]. Semi-analytical modeling of STPMMs considering the iron core relative permeability was applied by using subdomain technique and Taylor polynomial in [30].

In this research, we present a mathematical expression for determining the optimal radius of an iron pole in a STPMM. Also, an accurate analytical model for determining the performance characteristics of the machine is given by considering the iron core relative permeability at no-load and on-load conditions. In this model, the iron core relative permeability and the optimum curvature radius of the rotor pole are considered. The proposed model is based on the formal resolution of the Laplace's and Poisson's equations in different regions of the machine by using the separation of variables method and hyperbolic functions in a quasi-Cartesian coordinate system and applying boundary conditions (BCs) and interface conditions (ICs). In the proposed quasi-Cartesian coordinate system, the t and θ coordinates are used to express the coordinates of different regions. Thus, in the final model machine performances characteristics, functions are expressed as hyperbolic. Then, the models presented in this system are mathematically simple and the coefficients can be easily determined. It is easy to apply mathematical functions to different parameters. The effect of PM width on the optimal curvature radius of an iron pole has been investigated. Also, the machine's performance has been studied for different values of magnet widths and iron core relative permeability. In order to validate the results, three STPMMs are considered as case studies and the effect of the optimal radius of the iron pole is analytically and numerically compared.

2 Subdomain Definition, Assumptions, and Equations

In Fig. 1, an example of an STPM machine is shown with the region symbols described in Table 1. The machine regions can be defined as periodic or non-periodic regions. Table 1 lists the different regions of the studied machine. In Table 2, the periodic and non-periodic regions and the general PDE equations of each region are derived.

Analytical model in the Cartesian pseudo-coordinate system is formulated by the resolution of the Laplace's and Poisson's equations for determining the magnetic potential as A = {0; 0; A_z}. In the solution of the Maxwell equations, we use the following simplifying assumptions.

1. The axial length of the machine is assumed to be infinitely and the magnetic variables independent of z.
2. Stator teeth/slots, the rotor regions have radial sides.
3. The current density, J_z, is along the z axis.
4. It is assumed that the electrical conductivity of the material is zero.

Field vectors $B = \{B_t; B_\theta; 0\}$ and $H = \{H_t; H_\theta; 0\}$ are coupled in different regions by means of magnetic material equation as shown in Table 3.

Using $B = \nabla\times A$ the components of B can be deduced by

$$B_t = \frac{e^t}{R_i}\frac{\partial A_z}{\partial \theta} \tag{1}$$

and

$$B_\theta = \frac{e^t}{R_i}\frac{\partial A_z}{\partial t} \tag{2}$$

3 Resolutions of Laplace’s and Poisson’s Equations

First, periodic and non-periodic areas are determined in this section, and then the corresponding Laplace's or Poisson's equation is solved by the method of separation of the variables as listed in Table 4. In order to determine the constants of integration, the boundary conditions and the interface conditions are considered.

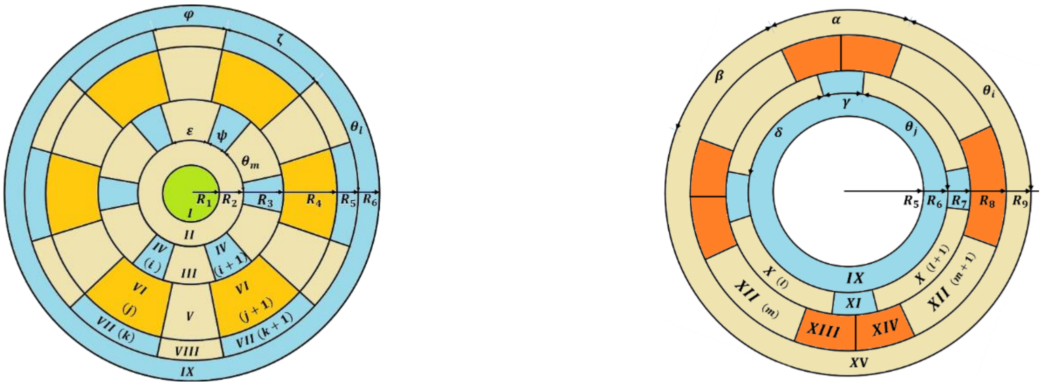

(a) (b)

Fig. 1 The investigated model; a) the rotor subdomains and b) the stator subdomains.

Table 1 Representation of the machine regions.

Symbol	Description	Symbol	Description
Region I	Rotor shaft	Region X and XII	Stator teeth
Region II	Rotor yoke	Region XI	Stator slot-opening
Region III	Rotor teeth	Region XIII	Stator slot (on the left)
Region IV	Rotor slot	Region XIV	Stator slot (on the right)
Region l	PMs	Region XV	Stator yoke
Region IX	Air-gap		

Table 2 Definition of periodic and non-periodic regions and their reprehensive Laplace’s or Poisson’s equation.

Category	Ω-Region	Laplace’s/ Poisson’s equation (μ_0 is the vacuum permeability; $\vec{M}$ is the magnetization of the PM; Jz is the current density in the stator slots)
Periodic region	I, II, XI, XV	$\nabla^2 A_z = \frac{\partial^2 A_\Omega}{\partial t^2} + \frac{\partial^2 A_\Omega}{\partial \theta^2} = 0$
Non-periodic region	III, IV, V, VIII, VII, X, XI, XII	
	VI	$\nabla^2 A_z = -\mu_0 \nabla\times M = \frac{\partial^2 A_{\Omega(g)}}{\partial t^2} + \frac{\partial^2 A_{\Omega(g)}}{\partial \theta^2} = -\mu_0 R_3 e^{-t} M_\theta$
	XIII and XIIV	$\nabla^2 A_z = -\mu_0 J = \frac{\partial^2 A_\Omega}{\partial t^2} + \frac{\partial^2 A_\Omega}{\partial \theta^2} = -\mu_0 R_7{}^2 e^{-2t} . J_{zi}$

Table 3 The magnetic material equation for each subdomain.

Region	Equation μ_{rm} is the relative recoil permeability of PMs and μ_{rc} is the relative recoil permeability of iron parts
I, IV, VII, XI, and XI	$\boldsymbol{B} = \mu_0\boldsymbol{H}$
VI	$\boldsymbol{B} = \mu_0\mu_{rm}\boldsymbol{H} + \mu_0\boldsymbol{M}$
II, III, V, VIII, X, XII and XV	$\boldsymbol{B} = \mu_0\mu_{rc}\boldsymbol{H}$

Table 4 General solution of Laplace's or Poisson's equation for each subdomain.

Ω-Region	General solution of Laplace's or Poisson's equation	Parameters definition
I, II, XI, XV	$A_{z\Omega}(t.\theta) = a_0^{\Omega} + b_0^{\Omega} t - f_{z\Omega}(t)$ $+\sum_{n=1}^{\infty}\left(a_n^{\Omega}\frac{F(n(t-t_j))}{Sh(n(t_i-t_j))} + b_n^{\Omega}\frac{F(n(t-t_i))}{Sh(n(t_j-t_i))}\right)\cos(n\theta)$ $+\sum_{n=1}^{\infty}\left(c_n^{\Omega}\frac{F(n(t-t_j))}{Sh(n(t_i-t_j))} + d_n^{\Omega}\frac{F(n(t-t_i))}{Sh(n(t_j-t_i))}\right)\sin(n\theta)$	for $\begin{cases} f_{z\Omega}(t) = 0 \\ \theta \in [0,\, 2\pi] \end{cases}$ where, *n* is a positive integer, $F = Sh$, $t \in [t_i = t_1,\, t_j = t_2]$ and $b_n^{\Omega} = d_n^{\Omega} = 0$ for (Ω = I), $F = Sh$ and $t \in [t_i = t_3,\, t_j = t_4]$, for (Ω = II), $F = Sh$, $t \in [t_i = t_{17},\, t_j = t_{18}]$ and $b_n^{\Omega} = d_n^{\Omega} = 0$ for (Ω = XV), $F = Ch$ and $t \in [t_i = t_{11},\, t_j = t_{12}]$ for (Ω = XI).
III, IV, V, VIII, VII, X, XI, XII	$A_{z\Omega(g)}(t.\theta) = a_0^{\Omega(g)} + b_0^{\Omega(g)} t - f_{z\Omega(g)}(t)$ $+\sum_{h=1}^{\infty}\left(\frac{a_h^{\Omega(g)}}{\nu_{h.\Omega(g)}}\frac{F(\nu_{h.\Omega(g)}(t-t_j))}{Sh(\nu_{h.\Omega(g)}(t_i-t_j))} + \frac{b_h^{\Omega(g)}}{\nu_{h.\Omega(g)}}\frac{F(\nu_{h.\Omega(g)}(t-t_i))}{Sh(\nu_{h.\Omega(g)}(t_j-t_i))}\right)\cos(\nu_{h.\Omega(g)}(\theta-\theta_1))$ $+\sum_{k=1}^{\infty}\left(\frac{a_k^{\Omega(g)}}{\nu_{k.\Omega(g)}}\frac{Sh(\nu_{k.\Omega(g)}(\theta-\theta_1))}{Sh(\nu_{k.\Omega(g)}\Theta)} + \frac{b_k^{\Omega(g)}}{\nu_{k.\Omega(g)}}\frac{Sh(\nu_{k.\Omega(g)}(\theta-\theta_2))}{Sh(\nu_{k.\Omega(g)}\Theta)}\right)\sin(\nu_{k.\Omega(g)}t)$	for $\begin{cases} f_{z\Omega(g)}(t) = 0 \\ \theta \in [\theta_1,\, \theta_2] \\ \nu_{h.\Omega(g)} = h\pi / \Theta \\ \nu_{k.\Omega(g)} = k\pi / t_j \end{cases}$ where, $t \in [t_{15},\, t_{16}]$, $\Theta = \beta$, $\theta \in [\theta_1,\, \theta_2] = [\theta i + \alpha,\, \theta_i + \alpha + \beta]$, Ω(*g*) = XII(*m*) and *F* = *Ch* for *m*-th stator teeth, $t \in [t_{13},\, t_{14}]$, $\Theta = \delta$, $\theta \in [\theta_j + \gamma,\, \theta_j + \gamma + \delta]$, Ω(*g*) = X(*l*) and *F*= *Ch* for *l*-th stator teeth, $t \in [t_{13},\, t_{14}]$, $\Theta = \gamma$, $\theta \in [\theta_j,\, \theta_j + \gamma]$, *F* = *Sh*, Ω(*g*) = *XI*(*l*) and $a_k^{\Omega(g)} = b_k^{\Omega(g)} = 0$ for *l*-th stator slot-opening, $t \in [t_9,\, t_{10}]$, $\Theta = \zeta$, $\theta \in [\theta_l,\, \theta_l + \zeta]$, $a_k^{\Omega(g)} = b_k^{\Omega(g)} = 0$, *F* = *Sh* and *Ω*(*g*) = VII(*k*) for *k*-th rotor outer slot, $t \in [t_9,\, t_{10}]$, $\Theta = \varphi$, $\theta \in [\theta_l + \zeta,\, \theta_l + \zeta + \varphi]$, *F* = *Ch* and *Ω*(*g*) = VIII(*k*) for *k*-th rotor teeth, $t \in [t_7,\, t_8]$, $\Theta = \varphi$, $\theta \in [\theta_l + \zeta,\, \theta_l + \zeta + \varphi]$, *F* = *Ch* and Ω(*g*) = *V*(*j*) for *j*-th rotor teeth, $t \in [t_5,\, t_6]$, $\Theta = \psi$, $\theta \in [\theta_m,\, \theta_m + \psi]$, $a_k^{\Omega(g)} = b_k^{\Omega(g)} = 0$, *F* = *Sh* and Ω(*g*)=IV(*i*) for *i*-th rotor inner slot, $t \in [t_5,\, t_6]$, $\Theta = \varepsilon$, $\theta \in [\theta_m + \psi,\, \theta_m + \psi + \varepsilon]$, *F* = *Ch* and Ω(*g*)=III(*i*) for *i*-th rotor teeth.
VI	$A_{z\Omega(g)}(t.\theta) = a_0^{\Omega(g)} + b_0^{\Omega(g)} t - f_{\Omega(g)}(t)$ $+\sum_{h=1}^{\infty}\left(\frac{a_h^{\Omega(g)}}{\nu_{h.\Omega(g)}}\frac{Ch(\nu_{h.\Omega(g)}(t-t_j))}{Sh(\nu_{h.\Omega(g)}(t_i-t_j))} + \frac{b_h^{\Omega(g)}}{\nu_{h.\Omega(g)}}\frac{Ch(\nu_{h.\Omega(g)}(t-t_i))}{Sh(\nu_{h.\Omega(g)}(t_j-t_i))} + X_h^{\,l}(t)\cos(\nu_{h.\Omega(g)}\varphi_i)\right)\cos(\nu_{h.\Omega(g)}(\theta-\theta_1))$ $+\sum_{k=1}^{\infty}\left(\frac{a_k^{\Omega(g)}}{\nu_{k.\Omega(g)}}\frac{Sh(\nu_{k.\Omega(g)}(\theta-\theta_1))}{Sh(\nu_{k.\Omega(g)}\Theta)} + \frac{b_k^{\Omega(g)}}{\nu_{k.\Omega(g)}}\frac{Sh(\nu_{k.\Omega(g)}(\theta-\theta_2))}{Sh(\nu_{k.\Omega(g)}\Theta)}\right)\sin(\nu_{k.\Omega(g)}t)$	for $\begin{cases} f_{\Omega(g)}(t) = R_3 e^{-t}(-1)^i B_r(\theta-\theta_1) \\ t \in [t_7,\, t_8] \\ \theta \in [\theta_1,\, \theta_2] = [\theta_l,\, \theta_l + \zeta] \\ \nu_{h.\Omega(g)} = h\pi / \Theta \\ \nu_{k.\Omega(g)} = k\pi / t_j \\ \Theta = \zeta \\ \Omega(g) = VI(j) \end{cases}$
XIII and XIIV	$A_{z\Omega(g)}(t.\theta) = a_0^{\Omega(g)} + b_0^{\Omega(g)} t - f_{\Omega(g)}(t)$ $+\sum_{h=1}^{\infty}\left(\frac{a_h^{\Omega(g)}}{\nu_{h.\Omega(g)}}\frac{Ch(\nu_{h.\Omega(g)}(t-t_j))}{Sh(\nu_{h.\Omega(g)}(t_i-t_j))}\right)\cos(\nu_{h.\Omega(g)}(\theta-\theta_1))$ $+\sum_{k=1}^{\infty}\left(\frac{a_k^{\Omega(g)}}{\nu_{k.\Omega(g)}}\frac{Sh(\nu_{k.\Omega(g)}(\theta-\theta_1))}{Sh(\nu_{k.\Omega(g)}\Theta)} + \frac{b_k^{\Omega(g)}}{\nu_{k.\Omega(g)}}\frac{Sh(\nu_{k.\Omega(g)}(\theta-\theta_2))}{Sh(\nu_{k.\Omega(g)}\Theta)}\right)\sin(\nu_{k.\Omega(g)}t)$	for $\begin{cases} f_{z\Omega(g)}(t) = \frac{1}{4}\mu_0 J_{z\Omega(g)} e^{-2t} \\ \theta \in [\theta_1,\, \theta_2] \\ t \in [t_i,\, t_j] = [t_{15},\, t_{16}] \\ \Theta = \alpha / 2 \\ \nu_{h.\Omega(g)} = h\pi / \Theta \\ \nu_{k.\Omega(g)} = k\pi / t_j \end{cases}$ where, $\theta \in [\theta_i,\, \theta_i + \alpha/2]$ and Ω(*g*) = XIII(*m*) for *m*-th stator slot-right side and $\theta \in [\theta_i + \alpha/2,\, \theta_i + \alpha]$ and Ω(*g*) = XIV(*m*) for *m*-th stator slot-left side.

The main idea in pulsating torque reduction is to change the pole shape. The following analytical expression is considered in order to determine the optimal iron pole shape in the pseudo-Cartesian coordinate system [17]:

$$t_{opt}\left(\theta\right)=F^{-1}\left\{\frac{F\left(t_5\right)}{Cos\left(\theta\right)}\right\}+t_5 \tag{3}$$

The relation between optimal iron pole radii R_{opt} and θ is given by

$$R_{opt}\left(\theta\right)=\frac{R_1}{\exp\left(F^{-1}\left\{\frac{F\left(t_5\right)}{Cos\left(\theta\right)}\right\}+t_5\right)} \tag{4}$$

where F = Cosh.

4 Interface Condition Between Regions

To determine the integration constants in (9)-(12), the boundary conditions at the interface between the different regions should be introduced. In non-homogenous regions, we consider the interface conditions in two edges (i.e., t- and θ–edges) are given in Table 5.

5 Results and Evaluation

In order to study the effect of magnet width on the optimal iron pole shape, an 8P-18S spoke type machine with three different magnet widths (viz. 5 mm, 16 mm, and 17.5 mm) has been modeled analytically, numerically and experimentally. The two-dimensional analytical representation for STPM machine, considering the rotor iron pole shape and distinct material permeability is applied to estimate the machine performances. The main dimensions and parameters of the investigated STPM machine are given in Table 6. Initial and optimal iron pole shapes represented to each design (i.e. M1 with w = 5 mm, and M3 with w = 17.5 mm PM width) are respectively shown in Figs. 2 and 3.

Table 5 t and θ-edges interface conditions.

θ-edges ICs		t-edges ICs	
$A_{z\Omega}\big\|_{t=t_i}=A_{z\Psi}\big\|_{t=t_j}$ and $H_{\theta\Omega}\big\|_{t=t_i}=H_{\theta\Psi}\big\|_{t=t_j}$		$A_{z\Omega}\big\|_{\theta}=A_{z\Psi}\big\|_{\theta}$ and $H_{t\Omega}\big\|_{\theta}=H_{t\Psi}\big\|_{\theta}$	
$R = R_2$	$\forall\,\theta \in [\theta_l, \theta_l + \zeta]$ between Region Ω = II at t_4/Region Ψ = IV(i) at t_5 and $\forall\,\theta \in [\theta_l + \zeta, \theta_l + \zeta + \varphi]$ between Region Ω = II/Region III(i).	$\forall\, t \in [t_3, t_4]$	at $\theta = \theta_m$ between Region IV(i)/Region III(i) and $\theta = \theta_m + \psi$ between Region IV(i)/Region III(i).
$R = R_3$	$\forall\,\theta \in [\theta_m + \psi, \theta_m + \psi + \varepsilon]$ between Region Ω = V at t_7/Region Ψ = III(i) at t_6 and $\forall\,\theta \in [\theta_m, \theta_m + \varphi]$ between Region Ω = VI(j)/Region Ψ = IV(i).	$\forall\, t \in [t_5, t_6]$	at $\theta = \theta_l$ between Region VI(i)/Region V(i) and $\theta = \theta_l + \zeta$ between Region VI(i)/Region V(i).
$R = R_4$	$\forall\,\theta \in [\theta_l + \zeta, \theta_l + \zeta + \varphi]$ between Region V(j) at t_8/Region VIII(k) at t_9 and $\forall\,\theta \in [\theta_l, \theta_l + \zeta]$ between Region VI(j)/Region VII(k).	$\forall\, t \in [t_7, t_8]$	at $\theta = \theta_l$ between Region VI(j)/Region V(j) and $\theta = \theta_l + \zeta$ between Region VI(j)/Region V(j).
$R = R_5$	$\forall\,\theta \in [\theta_l + \zeta, \theta_l + \zeta + \varphi]$ between Region IX at t_{11}/Region VIII(k) at t_{10} and $\forall\,\theta \in [\theta_l, \theta_l + \zeta]$ between Region IX/Region VII(k).	$\forall\, t \in [t_9, t_{10}]$	at $\theta = \theta_l$ between Region VII(k)/Region VIII(k) and at $\theta = \theta_l + \zeta$ between Region VII(k)/Region VIII(k).
$R = R_6$	$\forall\,\theta \in [\theta_j + \gamma, \theta_j + \gamma + \delta]$ between Region IX at t_{12}/Region X(l) at t_{13} and $\forall\,\theta \in [\theta_j, \theta_j + \gamma]$ between Region IX/Region XI(l).	$\forall\, t \in [t_{13}, t_{14}]$	at $\theta = \theta_j$ between Region XI(l)/Region X(l) and $\theta = \theta_j + \gamma$ between Region XI(l)/Region X(l).
$R = R_7$	$\forall\,\theta \in [\theta_j, \theta_j + \gamma/2]$ between Region XI(l) at t_{14}/Region XIII(m) at t_{15}, $\forall\,\theta \in [\theta_j + \gamma/2, \theta_j + \gamma]$ Region XI at t_{14}/Region XIV at t_{15}, $\forall\,\theta \in [\theta_i + \alpha, \theta_i + \alpha + \beta]$ between Region XII(m) at t_{15}/Region X(l) at t_{14}, $\forall\,\theta \in [\theta_j, \theta_j + \gamma]$ between Region X(l) at t_{14}/Region XIII(m) at t_{15}, $\forall\,\theta \in [\theta_j + \gamma, \theta_i + \alpha]$ between Region X(l+1) at t_{14}/Region XIII(m+1) at t_{15}, and $\forall\,\theta \in [\theta_j, \theta_j + \gamma]$ between Region XI at t_{14}/Region XIV at t_{15}.	$\forall\, t \in [t_{15}, t_{16}]$	at $\theta = \theta_i$ between Region XIII(m)/Region XII(m), at $\theta = \theta_i + \alpha/2$ between Region XIV(m)/Region XIII(m), $\theta = \theta_i + \alpha$ between Region XIV(m)/Region XII(m).
$R = R_8$	$\forall\,\theta \in [\theta_i + \alpha, \theta_i + \alpha + \beta]$ between Region XV at t_{17}/Region XII(m) at t_{16} and $\forall\,\theta \in [\theta_i, \theta_i + \alpha/2]$ between Region XV at t_{17}/Region XIII(m) at t_{16}, $\forall\,\theta \in [\theta_i + \alpha/2, \theta_i + \alpha]$ between Region XV at t_{17}/Region XIV(m) at t_{16} .		

Table 6 Parameters of the studied machines.

Symbol	Parameters	Value	Unit	Symbol	Parameters	Value	Unit
B_{rm}	Remanence flux density of PMs	1	T	R_4	Outer radius of stator slots	60.3	mm
μ_{rm}	Relative permeability of PMs	1		R_3	Radius of the stator inner surface	45.3	mm
N_c	Number of conductors per stator slot	120		R_2	Radius of the rotor outer surface at the PM surface	44.8	mm
I_m	Peak phase current	10	A	R_1	Radius of the rotor inner surface at the PM bottom	18	mm
Q_s	Number of stator slots	6		g	Air-gap length	0.5	mm
c	Stator slot-opening	30	deg.	L_u	Axial length	57	mm
a	PM opening	18	deg.	n	Mechanical pulse of synchronism	10000	rpm
p	Number of pole pairs	2					

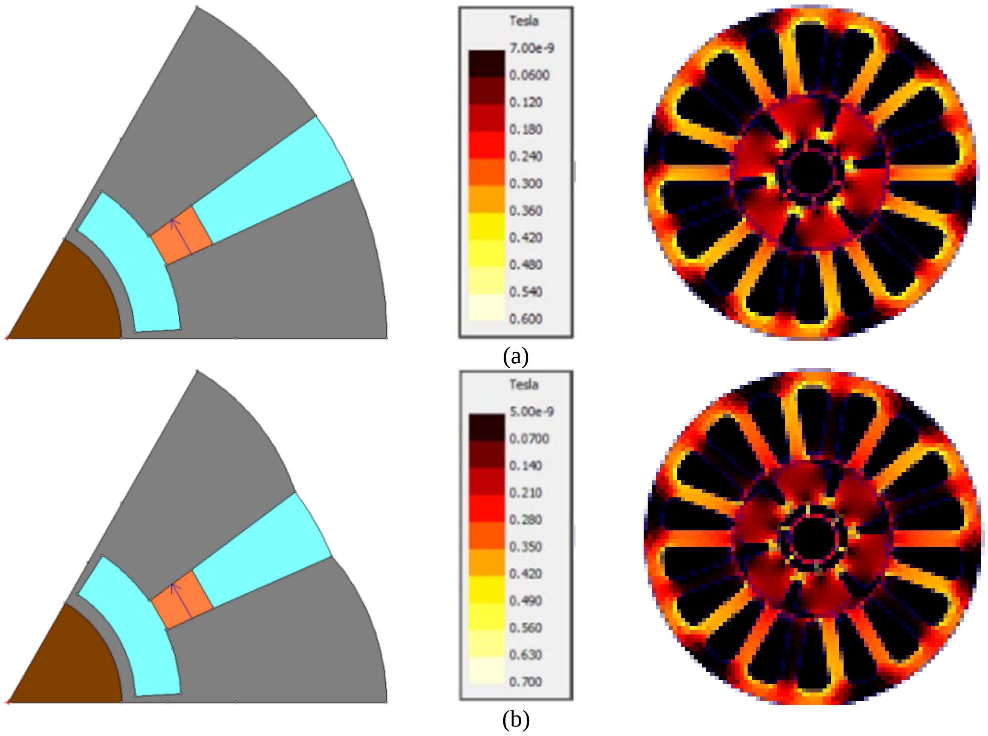

Fig. 2 M1 design (w = 5 mm); a) initial shape and b) optimal shape.

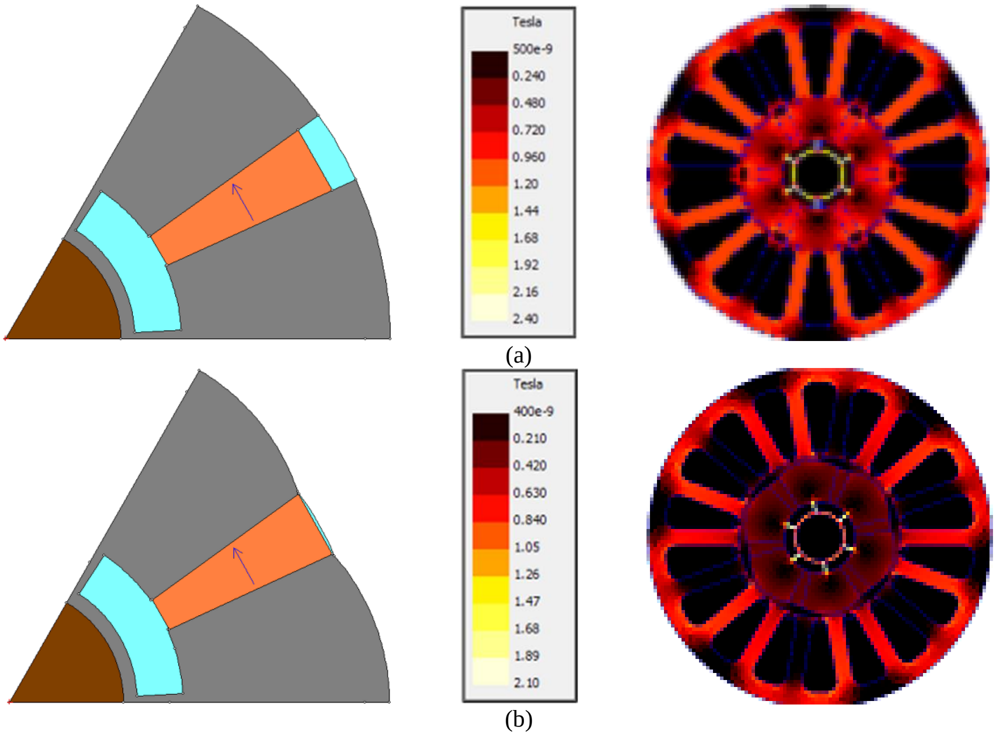

Fig. 3 M3 design (w = 17.5 mm); a) initial shape and b) optimal shape.

The fabricated spoke type motor and experimental test setup are shown in Fig. 4. To measure the cogging torque, the rotor shaft should turn without any input current. To perform this, the rotor is turned with the help of an auxiliary motor. The torque which is caused by the rotation of the rotor is measured by the torque sensor which is mounted underneath the housing of the motor. The position is measured by the digital encoder. At the defined speeds data from 24 revolutions is saved. The number of revolutions is bounded by the maximum amount of data which can be sampled in one trial.

The electromagnetic performances for the initial and optimal shape of different machines (i.e., M1 with w = 5 mm, M2 with w = 16 mm, and M3 with w = 17.5 mm) at no-load and on load conditions are compared analytically and numerically in Fig. 5 and 6 (for M1), in Fig. 7 and 8 (for M2), and in Fig. 9 and 10 (for M3). The maximum error percentage of these results is 4.3% for M1, 4.4% for M2, and 4.7% for M3.

Fig. 4 Experimental test setup.

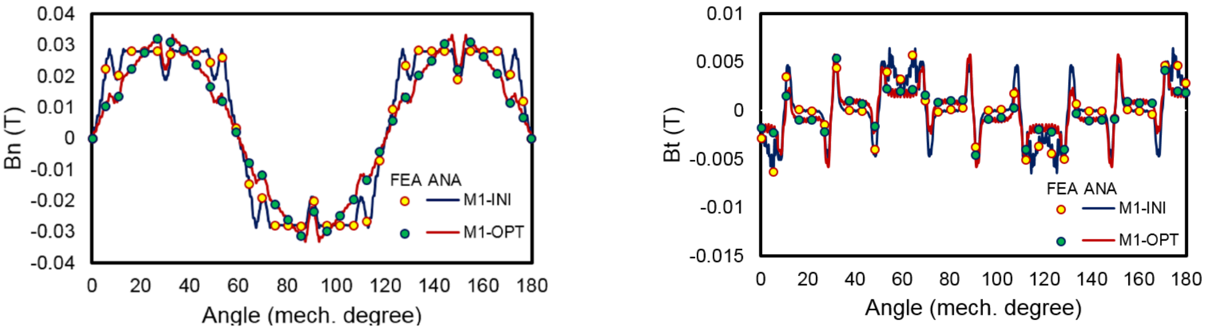

(a) (b)

Fig. 5 No-load performances for M1 design with w = 5 mm; a) radial flux density and b) tangential flux density.

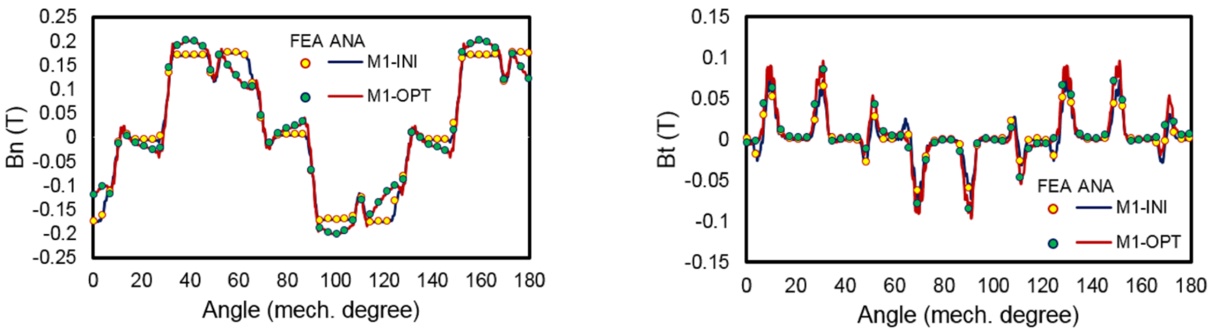

(a) (b)

Fig. 6 On-load performances for M1 design with w = 5 mm; a) radial flux density and b) tangential flux density.

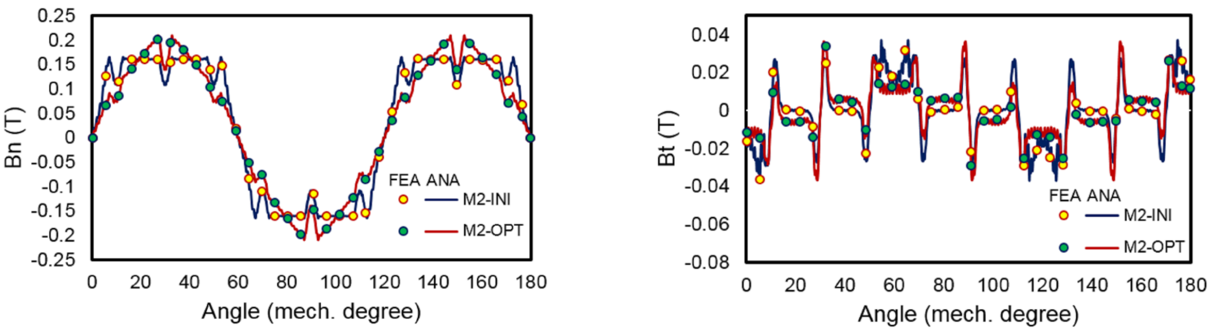

(a) (b)

Fig. 7 No-load performances for M2 design with w = 16 mm; a) radial flux density and b) tangential flux density.

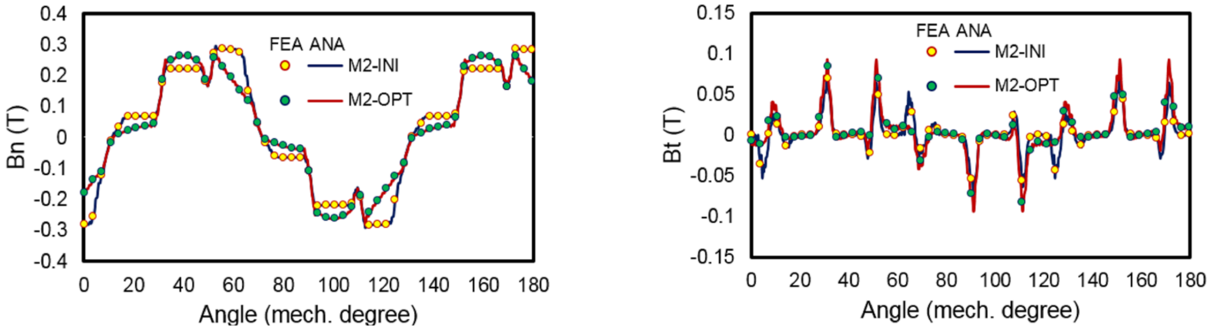

(a) (b)

Fig. 8 On-load performances for M2 design with w = 16 mm; a) radial flux density and b) tangential flux density.

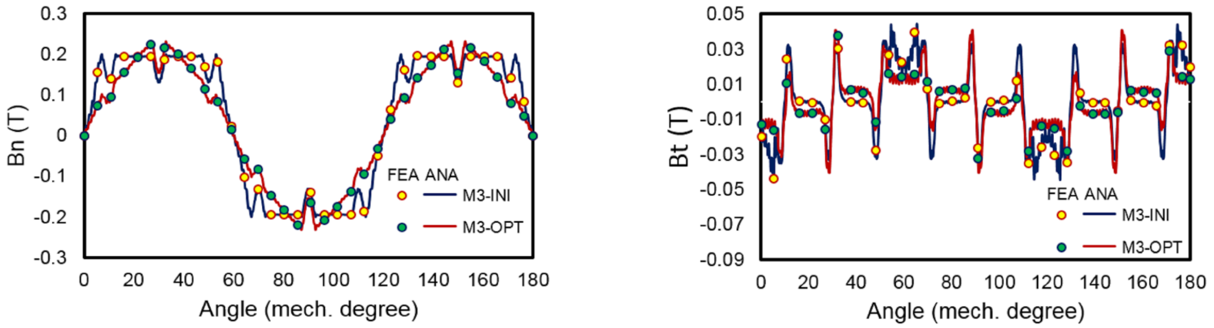

(a) (b)

Fig. 9 No-load performances for M3 design with w = 17.5 mm; a) radial flux density and b) tangential flux density.

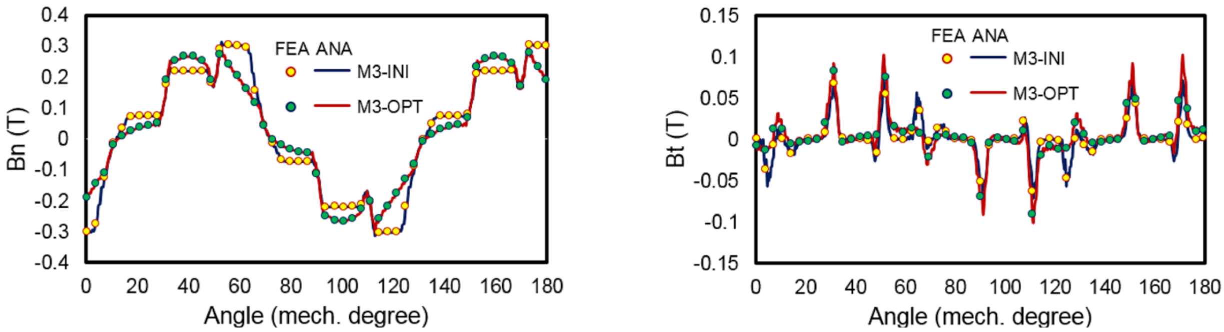

(a) (b)

Fig. 10 On-load performances for M3 design with w = 17.5 mm; a) radial flux density and b) tangential flux density.

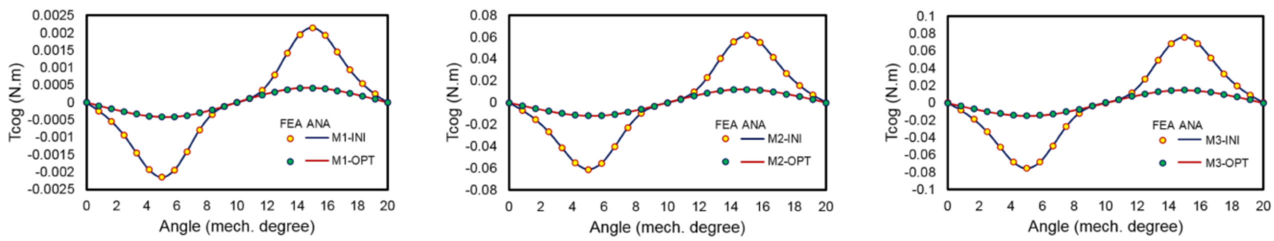

(a) (b) (c)

Fig. 11 Cogging torque waveforms for (a) M1-design, (b) M2-design and (c) M3-design.

Fig. 11 represent the cogging torque waveforms with the initial and optimal shape for different machines. As shown in Table 7, the peak value of the cogging torque after optimization in M1, M2, and M3 is reduced to 80.8012%, 80.5834%, and 80.507%, respectively.

The average and ripple of the electromagnetic torque, of the reluctance torque, the peak back-EMF, the self- and mutual inductances for the three values of iron core

Table 7 A cogging torque comparison for different designs.

Type	Initial design	Optimal design	%
M1	0.002151	0.000413	−80.8012
M2	0.061338	0.01191	−80.5834
M3	0.075809	0.014778	−80.507

relative permeability for the initial and optimal designs are given in Table 8. Also, the amount of increase or decrease of each parameter for the optimal design compared to the original design is presented in this table. For example, the electromagnetic torque ripple for the iron permeability of infinite and 800, respectively, is reduced by 36.55% and 25.89%, and for iron permeability of 200, it increases by 3.77%. From the results of the study, it can be seen that in the optimum machine compared with the original design, for iron permeability values of infinity, 800, and 200, the reluctance torque ripple reduced by 38.79, 26.85, and 26.2%, respectively.

A remarkable point is that after shape optimizing, the mean electromagnetic torque and the mean reluctance torque values increase for three iron core relative permeability values. This is despite the fact that the back-EMF amplitude decreases for the three iron permeability after the optimization process.

A performance comparison between the initial and optimal shape is shown in Fig. 13 for M2 machine. Electromagnetic torque, reluctance torque, back-EMF, and self-/mutual-inductance of the two machines are compered analytically and numerically.

A performance comparison between the initial and optimal design is shown in Fig. 12. Electromagnetic torque, reluctance torque, back-EMF, and self-/mutual-inductance of the two machines are compered

Table 8 Machine characteristics at three different soft magnetic relative permeability.

Machine characteristic	Initial design			Optimal design			Amount of increase/decrease [%]		
	$\mu = \infty$	$\mu = 800$	$\mu = 200$	$\mu = \infty$	$\mu = 800$	$\mu = 200$	$\mu = \infty$	$\mu = 800$	$\mu = 200$
Average electromagnetic torque	0.212954	0.106282	0.054748	0.513701	0.230502	0.109225	141.2263	116.8773	99.50591
Electromagnet torque ripple	0.410832	0.192496	0.072371	0.260668	0.142666	0.074687	−36.5512	−25.8861	3.200177
Average reluctance torque	0.175799	0.079272	0.007512	0.477472	0.19576	0.04515	171.6007	146.9461	501.0157
Reluctance torque ripple	0.413152	0.195476	0.050422	0.252112	0.142987	0.037211	−38.9783	−26.8518	−26.201
Back-emf	0.68199	3.4217	15.442	0.6669	3.1362	13.0628	−15.4073	−8.34381	−2.21264
Self-inductance	0.000668	0.000665	0.000644	0.000559	0.000557	0.000543	−16.3346	−16.2932	−15.7082
Mutual inductance	−0.00016	−0.00016	−0.00015	−0.0001	−0.0001	−0.0001	−34.0233	−33.5181	−32.4349

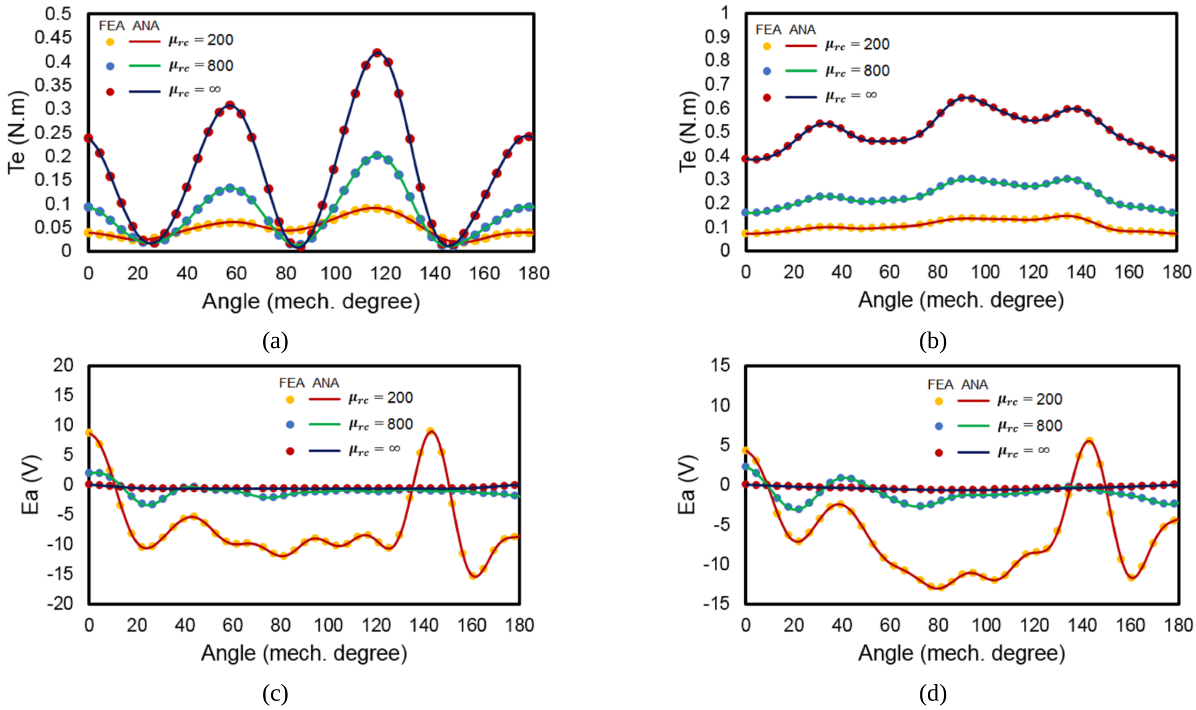

Fig. 12 A performance comparison between initial and optimal designs, initial design-left side, optimal design-right side; a) Electromagnetic torque-initial design, b) Electromagnetic torque-optimal design, c) Phase A Back-EMF-initial design, and d) Phase A Back-EMF-optimal design.

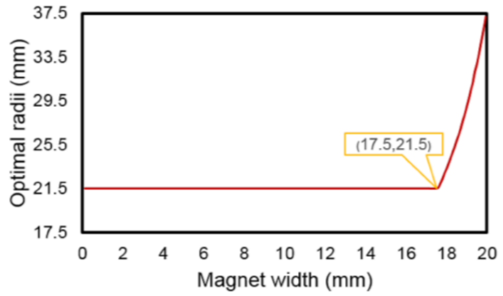

Fig. 13 The effect of magnet width on optimal radii in the investigated machine.

analytically and numerically.

Fig. 13 shows the effect of the magnet width on the optimal radius of the rotor pole in the investigated permanent magnet spoke-type machine. As you can see, in the widths of the magnet less than 17.5 mm, the optimal radius of the iron pole is independent of the width of the magnet and its value is 21.5 mm. Meanwhile, with an increase in the width of the magnet to 20 mm, the radius of the optimal curvature of the iron pole is approximately linearly with the relation

$$R_{opt}(w)=\begin{cases} R_{opt}(\theta) & w \le 17.5mm \\ R_{opt}(\theta)+0.8w & w > 17.5mm \end{cases} \tag{5}$$

where w is magnet width in mm.

6 Conclusion

In this paper, we present a semi-analytical method for calculating the optimal radius of the rotor's iron pole in permanent magnet spoke-type machines. In addition, the effect of magnet width and relative permeability of iron core on the optimal radius of iron pole was studied, analytically and numerically. From the results of this study, it can be observed that although the iron core relative permeability is effective on the peak values of the pulsating torque components of the machine, but does not affect the optimal radius of the iron pole. Also, for the values below the magnet width at the optimal point, the optimal radius is constant and independent of the width of the magnet, and in larger quantities, the radius of the curvature of the iron pole is increased proportional to the width of the magnet. For validation of the proposed analytical model, the optimal radius of the rotor pole in a spoke-type machine was investigated for different magnitudes of magnet width and numerical and analytical results were compared. Comparing these results, it can be seen that the proposed model is highly accurate.

Acknowledge

This research is carried out based on a research project which has been financially supported by the office of vice chancellor for research of Arak University with contact number of 98/3651.

References

[1] W. Zhao, T. A. Lipo, and B. I. Kwon, "Torque pulsation minimization in spoke-type interior permanent magnet motors with skewing and sinusoidal permanent magnet configurations," *IEEE Transactions on Magnetics*, Vol. 51, No. 11, pp. 1–4, Jun. 2015.

[2] A. Jabbari, M. Shakeri, and A. N. Niaki, "Iron Pole shape optimization of permanent magnet synchronous motors using an integrated method," *Advances in Electrical and Computer Engineering Journal*, Vol. 10, No. 1, pp. 48–55, 2010.

[3] A. Jabbari, "An experimental and finite element analysis of radii and skew effects on interior permanent magnet motors performance," *International Journal of Innovation and Applied Studies*, Vol. 2, No. 1, pp. 50–60, Jan. 2013.

[4] P. La Delfa, M. Hecquet, F. Gillon, and J. Le Besnerais, "Analysis of radial force harmonics in PMSM responsible for electromagnetic noise", in *International Conference on Ecological Vehicles and Renewable Energies (EVER)*, pp. 1–6, Apr. 2015.

[5] S. Jia, R. Qu, J. Li, Z. Fu, H. Chen, and L. Wu, "Analysis of FSCW SPM servo motor with static, dynamic and mixed eccentricity in aspects of radial force and vibration," in *Energy Conversion Congress and Exposition (ECCE)*, pp. 1745–1753, Sep. 2014.

[6] D. Y. Kim, J. K. Nam, and G. H. Jang, "Reduction of magnetically induced vibration of a Spoke-Type IPM motor using magnetomechanical coupled analysis and optimization," *IEEE Transactions on Magnetics*, Vol. 49, No. 9, pp. 5097–5105, Sep. 2013.

[7] K. Boughrara, R. Ibtiouen, and F. Dubas, "Analytical prediction of electromagnetic performances and unbalanced magnetic forces in fractional slot spoke-type permanent-magnet machines," in *XXII International Conference on Electrical Machines (ICEM)*, Lausanne, Switzerland, pp. 1366–1372, Sep. 2016.

[8] R. L. J. Sprangers, J. J. H. Paulides, B. L. J. Gysen, and E. A. Lomonova, "Magnetic saturation in semi-analytical harmonic modeling for electric machine analysis," *IEEE Transactions on Magnetics*, Vol. 52, No. 2, Feb. 2016.

[9] R. L. J. Sprangers, J. J. H. Paulides, B. L. J. Gysen, J. Waarma, and E. A. Lomonova, "Semi analytical framework for synchronous reluctance motor analysis including finite soft-magnetic material permeability," *IEEE Transactions on Magnetics*, Vol. 51, No. 11, p.8110504, Nov. 2015.

[10] K.Z. Djelloul, K. Boughrara, F. Dubas, and R. Ibtiouen, "Nonlinear analytical prediction of magnetic field and electromagnetic performances in switched reluctance machines," *IEEE Transactions on Magnetics*, Vol. 53, No. 7, p. 8107311, Jul. 2017.

[11] L. Roubache, K. Boughrara, F. Dubas, and R. Ibtiouen, "New subdomain technique for electromagnetic performances calculation in radial-flux electrical machines considering finite soft-magnetic material permeability," *IEEE Transactions on Magnetics*, Vol. 54, No. 4, pp. 1–15, 2018.

[12] A. Jabbari, M. Shakeri, and S. A. Nabavi Niaki, "Pole shape optimization of permanent magnet synchronous motors using the reduced basis technique," *Iranian Journal of Electrical and Electronic Engineering*, Vol. 6, No. 1, pp. 48–55, 2010.

[13] A. Jabbari, "2D Analytical Modeling of Magnetic Vector Potential in Surface Mounted and Surface Inset Permanent Magnet Machines," *Iranian Journal of Electrical and Electronic Engineering*, Vol. 13, No. 4, pp. 362–373, 2017.

[14] A. Jabbari, "Exact analytical modeling of magnetic vector potential in surface inset permanent magnet DC machines considering magnet segmentation," *Journal of Electrical Engineering*, Vol. 69, No. 1, pp. 39–45, 2018.

[15] A. Jabbari, "Analytical modeling of magnetic field distribution in inner rotor brushless magnet segmented surface inset permanent magnet machines," *Iranian Journal of Electrical and Electronic Engineering*, Vol. 14, No. 3, pp. 259–269, 2018.

[16] A. Jabbari, "Analytical modeling of magnetic field distribution in multiphase h-type stator core permanent magnet flux switching machines," *Iranian Journal of Science and Technology, Transactions on Electrical Engineering*, Vol. 43, No. 1, pp.389–401, 2019.

[17] A. Jabbari, "An analytical expression for magnet shape optimization in surface-mounted permanent magnet machines," *Mathematical and Computational. Applications*, Vol. 23, No. 4, pp. 1-17, 2018.

[18] A. Jabbari, "An analytical study on iron pole shape optimization in high-speed interior permanent magnet machines," *Iranian Journal of Science and Technology, Transactions on Electrical Engineering*, Vol. 44, No. 1, pp.169-174, 2020.

[19] A. Jabbari and F. Dubas, "A new subdomain method for performances computation in interior permanent-magnet (IPM) machines," *Iranian Journal of Electrical and Electronic Engineering*, Vol. 16, No. 1, pp. 26–38, Mar. 2020.

[20] H. Tiegna, Y. Amara, and G. Barakat, "Overview of analytical models of permanent magnet electrical machines for analysis and design purposes," *Mathematical and. Computational Simulations*, Vol. 90, pp. 162–177, Apr. 2013.

[21] M. Curti, J. J. H. Paulides, and E. A. Lomonova, "An overview of analytical methods for magnetic field computation," in *Tenth International Conference on Ecological Vehicles and Renewable Energies (EVER)*, Grimaldi Forum, Monaco, pp. 1–7, 2015.

[22] F. Dubas and K. Boughrara, "New scientific contribution on the 2-D subdomain technique in Cartesian coordinates: Taking into account of iron parts," *Mathematical and Computational. Applications*, Vol. 22, No. 1, p. 17, Feb. 2017.

[23] F. Dubas and K. Boughrara, "New scientific contribution on the 2-D subdomain technique in polar coordinates: Taking into account of iron parts," *Mathematical and Computational. Applications*, Vol. 22, No. 4, p. 42, Oct. 2017.

[24] P. D. Pfister, X. Yin, and Y. Fang, "Slotted permanent-magnet machines: General analytical model of magnetic fields, torque, eddy currents, and permanent-magnet power losses including the diffusion effect," *IEEE Transactions on Magnetics*, Vol. 52, No. 5, pp. 1–13, May 2016.

[25] T. Lubin, S. Mezani, and A. Rezzoug, "Two-dimensional analytical calculation of magnetic field and electromagnetic torque for surface inset permanent-magnet motors," *IEEE Transactions on Magnetics*, Vol. 48, No. 6, pp. 2080–2091, Jun. 2012.

[26] P. Liang, F. Chai, Y. Li, and Y. Pei, "Analytical prediction of magnetic field distribution in spoke-type permanent-magnet synchronous machines accounting for bridge saturation and magnet shape," *IEEE Transactions on Industrial Electronics*, Vol. 64, No. 5, pp. 3479–3488, May 2017.

[27] M. Pourahmadi-Nakhli, A. Rahideh, and M. Mardaneh, "Analytical 2- D model of slotted brushless machines with cubic spoke-type permanent magnets," *IEEE Transactions on Energy Conversion*, Vol. 33, No. 1, pp. 373–382, 2017.

[28] Z. Djelloul-Khedda, K. Boughrara, R. Ibtiouen, and F. Dubas, "Nonlinear analytical calculation of magnetic field and torque of switched reluctance machines," in *International Conference on Electrical Sciences and Technologies in Maghreb (CISTEM)*, Marrakesh, Morocco, pp. 1–8, Oct. 2016.

[29] Z. Djelloul-Khedda, K. Boughrara, F. Dubas, and R. Ibtiouen, "Nonlinear analytical prediction of magnetic field and electromagnetic performances in switched reluctance machines," *IEEE Transactions on Magnetics*, Vol. 53, No. 7, Jul. 2017.

[30] L. Roubache, K. Boughrara, F. Dubas, and R. Ibtiouen, "Semi-analytical modeling of spoke-type permanent-magnet machines considering the iron core relative permeability: Subdomain technique and Taylor polynomial," *Progress in Electromagnetic Research*, Vol. 77, pp. 85–101, Jul. 2017.

A. Jabbari was born in Shazand, Iran, in 1980. He received the B.Sc. degree from Iran University of Science and Technology (IUST) in 2002 and his M.Sc. and Ph.D. degrees both in Mechanical Engineering from Mazandran University in 2004 and 2009, respectively, with a focus on design and optimization of brushless DC permanent magnet machines for direct drive applications. He is currently an Assistant Professor with the Department of Mechanical Engineering, Arak University, Arak, Iran. Since 2014, he has been the Head of "Gearless Wind Turbine Project" team. His research interests include gearless wind turbine design, analytical modeling, PM machines, subdomain technique, friction stir welding, and metal forming.

F. Dubas was born in Vesoul, France, in 1978. He received the M.Sc. degree from the Université of Franche-Comté (UFC) in 2002 and the Ph.D. degree from the UFC in 2006, with a focus on the design and the optimization of high-speed surface-mounted permanent-magnet (PM) synchronous motor for the drive of a fuel cell air-compressor. He is currently an Associate Professor with the Département ENERGIE, FEMTO-ST Institute affiliated to the CNRS and jointly with the University Bourgogne Franche-Comté. From 2014 to 2016, he has been the Head of "Unconventional Thermal and Electrical Machines" Team. He is the Head of the "Electrical Actuators" group in the "Hybrid & Fuel Cell Systems, Electrical Machines (SHARPAC)" Team. He works with ALSTOM Transports (France), and RENAULT (France), where he is involved in the modeling, design, and optimization of electrical systems and, in particular, induction and PM synchronous (radial and/or axial flux) machines, creative problem solving, and electrical propulsion/traction. He has authored over 100 refereed publications and he holds a patent about the manufacturing of axial-flux PM machines with flux-focusing. Dr. Dubas received the Prize Paper Awards in the IEEE Conference Vehicle Power and Propulsion (VPPC) in 2005 as well as the Prize Presentation Awards in the 19th International Conference on Electrical Machines and Systems (ICEMS) in 2017. His research interests are applied mathematics, partial differential equations, separation of variables method, principle of superposition, (semi-)analytical modeling, subdomain technique, magnetic equivalent circuit, and electrical machines.